

Large-Scale Magnetic Fields in Magnetohydrodynamic Turbulence

Alexandros Alexakis

Laboratoire de Physique Statistique de l'École Normale Supérieure, UMR CNRS 8550, 24 Rue Lhomond,
75006 Paris Cedex 05, France

(Received 19 September 2012; published 21 February 2013)

High Reynolds number magnetohydrodynamic turbulence in the presence of zero-flux large-scale magnetic fields is investigated as a function of the magnetic field strength. For a variety of flow configurations, the energy dissipation rate ϵ follows the scaling $\epsilon \propto U_{\text{rms}}^3/\ell$ even when the large-scale magnetic field energy is twenty times larger than the kinetic energy. A further increase of the magnetic energy showed a transition to the $\epsilon \propto U_{\text{rms}}^2 B_{\text{rms}}/\ell$ scaling implying that magnetic shear becomes more efficient at this point at cascading the energy than the velocity fluctuations. Strongly helical configurations form nonturbulent helicity condensates that deviate from these scalings. Weak turbulence scaling was absent from the investigation. Finally, the magnetic energy spectra support the Kolmogorov spectrum $k^{-5/3}$ while kinetic energy spectra are closer to the Iroshnikov-Kraichnan spectrum $k^{-3/2}$ as observed in the solar wind.

DOI: [10.1103/PhysRevLett.110.084502](https://doi.org/10.1103/PhysRevLett.110.084502)

PACS numbers: 47.27.-i, 52.35.Ra, 95.30.Qd

One of the most fundamental questions that can be asked about an out-of-equilibrium system is the relation between the energy injection or dissipation rate ϵ , and the amplitude of the fluctuations u_ℓ . In hydrodynamic turbulence such estimates are clear and the desired relation comes from the balance between the injection rate and the flux of energy to the small scales due to nonlinear interactions. Such considerations lead to the strong turbulence scaling

$$\epsilon \propto Cu_\ell^2/\tau_{\text{nl}} \propto Cu_\ell^3/\ell_F \quad (1)$$

for $\text{Re} \propto u_\ell \ell_F/\nu \gg 1$ [1,2]. Here ν is the kinematic viscosity, u_ℓ is the amplitude of the velocity fluctuations at the scale ℓ , and $\tau_{\text{nl}} = \ell/u_\ell$ the eddy turn over time (or else the nonlinear time scale). The index F indicates that the quantity is measured at the forcing scale. Constancy of the energy flux over all scales ℓ leads to $u_\ell \propto \epsilon^{1/3} \ell^{1/3}$ that results in the Kolmogorov (K41) prediction for the energy spectrum $E(k) \propto \epsilon^{2/3} k^{-5/3}$ [3].

The situation becomes more complex when linear wave terms are present introducing new time scales in the system. Magnetohydrodynamic (MHD) turbulence is such an example for which turbulent eddies and (Alfvén) waves coexist with many applications in industrial and astrophysical flows [4,5]. When a flow is coupled to a uniform magnetic field B_0 fluctuations travel parallel or antiparallel to the magnetic field lines with crossing time $\tau_A \propto \pm \ell_{\parallel}/B_0$. (The indexes \perp , \parallel indicate the direction perpendicular and parallel to the magnetic field, respectively.) Depending on the ratio τ_{nl}/τ_A different regimes of turbulence are expected [6–8]. If $\tau_{\text{nl}}/\tau_A \ll 1$ the role of the waves becomes insignificant and one returns to the Kolmogorov scaling relation (1). If however $\tau_{\text{nl}}/\tau_A \gg 1$ the scaling is modified due to the sweeping effect (see Ref. [6]). Then the system can be treated

within the framework of wave turbulence theory [9]. Phenomenological arguments with $(\ell_{\perp} \sim \ell_{\parallel} \sim \ell)$ lead to the relation

$$\epsilon \propto C \frac{u_\ell^2}{\tau_{\text{nl}}} \left(\frac{\tau_A}{\tau_{\text{nl}}} \right) \propto C \frac{u_{\ell_F}^4}{B_0 \ell_F}. \quad (2)$$

Constancy of energy flux over all scales then leads to the isotropic Iroshnikov-Kraichnan spectrum $E(k) \propto (\epsilon B_0)^{1/2} k^{-3/2}$ [10,11]. However isotropy is not a valid assumption. Using $\tau_{\text{nl}} \sim \ell_{\perp}/u_\ell$ in Eq. (1) and restricting to modes for which the turbulence is strong ($\tau_{\text{nl}} \lesssim \tau_A$) the anisotropic energy spectrum $E(k) \propto \epsilon^{2/3} k_{\perp}^{-5/3}$ with $k_{\parallel} \leq \epsilon^{1/3} k_{\perp}^{2/3}/B_0$ is obtained [12]. Assuming the proportionality coefficient to depend on scale $C \propto \ell_{\perp}^{1/4}$ in Eq. (1), an anisotropic Iroshnikov-Kraichnan spectrum $E(k) \propto \epsilon^{2/3} k_{\perp}^{-3/2}$ can be obtained [13]. If instead we make the same substitutions for τ_{nl} and τ_A in Eq. (2) (see Ref. [14]) we obtain the weak turbulence spectrum $E(k) \propto f(k_{\parallel}) k_{\parallel}^{1/2} (\epsilon B_0)^{1/2} k_{\perp}^{-2}$ (see Ref. [15] for exact result).

These spectra have been tested by direct numerical simulations (DNSs) in periodic boxes with a nonzero magnetic flux through one side ($\Phi = \int \mathbf{b} \cdot d\mathbf{s} \neq 0$). In strong turbulence, agreement on the exponent of spectrum has not been reached [16,17]. The weak turbulence spectrum has been produced in DNSs only when the $k_{\parallel} = 0$ modes are not forced [18,19]. If they are forced and $B_0/L \gg u_\ell/\ell$ then the system becomes quasi-2D with an inverse cascade of energy (thus neither relation (1) or (2) applies) [20]. In all regimes (strong, weak, and quasi-2D) the principle role for cascading the energy is played by the weakly varying modes in the direction of B_0 , and thus the observed scaling depends on L and ℓ_F .

The sensitivity of the dynamics on the forcing length and box size poses questions on the applicability of these results in more realistic flows with magnetic fields B_L that vary over large length scales L . B_L is typically approximated as uniform provided that the turbulent energy remains in much smaller scales. The validity of this approximation, however, is in doubt since small scale variations $\ell_\perp \ll L$ couple to large-scale parallel variations $\ell_\parallel \sim B_L \ell_\perp / u_\ell$. If B_L is strong enough, ℓ_\parallel can be as large as L and thus turbulence can depend on the topology of the large-scale magnetic fields. As a result, based on the value B_L alone we cannot *a priori* decide if turbulence falls in the weak, strong, or a quasi-2D turbulence regime. Another drawback of modeling large-scale fields as uniform fields is that triple periodic boxes with finite magnetic flux do not conserve magnetic helicity, one of the invariants of the ideal MHD equations. For these reasons, MHD turbulence with zero-flux large-scale fields needs to be investigated.

TABLE I. Table with the parameters of all runs. The numbers in the first four columns are the input parameters given by $\mathcal{G} \equiv \langle \mathbf{F}_u^2 \rangle^{1/2} / \nu^2 k_u^3$ the Grashof number, $\mathcal{M} \equiv \langle \mathbf{F}_b^2 \rangle^{1/2} / \langle \mathbf{F}_u^2 \rangle^{1/2}$ the ratio of magnetic to mechanical forcing, $\mathcal{H} \equiv \langle \mathbf{F}_b \cdot \nabla \times \mathbf{F}_b \rangle / \langle \mathbf{F}_b^2 \rangle k_b$ the relative helicity of the forcing and $\text{St} \equiv \tau_f / \tau$ the Strouhal number where $\tau_f \equiv 1 / (\langle \mathbf{F}_u^2 \rangle k_u^2)^{1/4}$. $\mathcal{M} = 0$ imply dynamo runs. The Prandtl number $\text{Pr} \equiv \nu / \eta$ for all runs was set equal to 1. The last columns give the measured parameters $\text{Re} \equiv \langle \mathbf{u}^2 \rangle^{1/2} / \nu k_u$ the Reynolds number and $\mathcal{R}_\lambda \equiv \langle \mathbf{u}^2 \rangle^{1/2} / \nu (\langle \nabla \times \mathbf{u} \rangle^2)^{1/2}$ the Taylor Reynolds number. $\mathcal{R}_\lambda \equiv \langle \mathbf{u}^2 \rangle^{1/2} \lambda / \nu$ (with $\lambda^2 \equiv \langle \mathbf{u}^2 \rangle / \langle (\nabla \times \mathbf{u})^2 \rangle$) the Taylor Reynolds number. The last column gives the range of values obtained by $\mu \equiv E_M / E_K$, the ratio of magnetic to kinetic energy. The simulations named A1–A13 were carried out in a grid of size 512^3 while the simulations named B1–B3 were carried out in a grid of size 1024^3 . The third 1024^3 -grid simulation started with the parameters of B3' and run up to $t \approx 24$ turn over times $\tau_u \equiv 1 / k_u \langle \mathbf{u}^2 \rangle^{1/2}$. afterwards it was continued with the parameters B3.

| Runs | $\mathcal{G}^{1/2}$ | \mathcal{M} | \mathcal{H} | St^{-1} | Re | \mathcal{R}_λ | μ |
|------|---------------------|---------------|---------------|------------------|------|-----------------------|-----------|
| A1 | 356 | 0.00 | ... | 0.50 | 580 | 157 | 0.4 |
| A2 | 1666 | 0.10 | 0.59 | 0.01 | 905 | 181 | 0.7 |
| A3 | 2500 | 0.00 | ... | 0.01 | 1331 | 206 | 0.7 |
| A4 | 1666 | 1.00 | 0.00 | 0.01 | 1064 | 170 | 1.4–1.7 |
| A5 | 353 | 0.50 | 0.15 | 0.50 | 541 | 106 | 1.5–2.9 |
| A6 | 353 | 0.50 | 0.31 | 0.50 | 690 | 151 | 2.4–3.2 |
| A7 | 353 | 0.50 | 1.00 | 0.50 | 734 | 205 | 2.6–4.5 |
| A8 | 353 | 0.50 | 0.95 | 0.50 | 645 | 148 | 2.7–5.0 |
| A9 | 353 | 1.00 | 0.15 | 0.50 | 811 | 141 | 1.8–7.6 |
| A10 | 1666 | 1.00 | 1.00 | 0.01 | 972 | 154 | 1.8–9.5 |
| A11 | 1666 | 1.00 | 0.59 | 0.01 | 920 | 138 | 2.0–14.0 |
| A12 | 1666 | 1.00 | 1.00 | 0.01 | 1877 | 634 | 5.7–12.0 |
| A13 | 1054 | 10.00 | 0.59 | 0.01 | 1081 | 105 | 6.0–94.0 |
| B1 | 3846 | 0.00 | ... | 0.01 | 2813 | 296 | 0.6 |
| B2 | 1414 | 0.50 | 0.31 | 0.5 | 2572 | 311 | 2.6 |
| B3' | 6123 | 1.00 | 1.00 | 0.01 | 3714 | 386 | 5.0–18.0 |
| B3 | 6123 | 0.40 | 0.50 | 0.01 | 4105 | 298 | 18.0–24.0 |

To study MHD turbulence in the presence of large-scale magnetic fields we employ high resolution direct numerical simulations of the MHD equations:

$$\partial_t \mathbf{u} + \mathbf{u} \cdot \nabla \mathbf{u} = \mathbf{b} \cdot \nabla \mathbf{b} - \nabla P + \nu \nabla^2 \mathbf{u} + \mathbf{F}_u, \quad (3)$$

$$\partial_t \mathbf{b} + \mathbf{u} \cdot \nabla \mathbf{b} = \mathbf{b} \cdot \nabla \mathbf{u} + \eta \nabla^2 \mathbf{b} + \mathbf{F}_b, \quad (4)$$

in a triple periodic box of size $L = 2\pi$. Here \mathbf{u} is the velocity field and \mathbf{b} the magnetic field. Both fields satisfy $\nabla \cdot \mathbf{u} = \nabla \cdot \mathbf{b} = 0$ and $\langle \mathbf{u} \rangle = \langle \mathbf{b} \rangle = 0$, where the angular brackets stand for spatial average. ν is the viscosity and η the magnetic diffusivity. \mathbf{F}_u is an external mechanical body force, while $\mathbf{F}_b = \nabla \times \mathcal{E}$ where \mathcal{E} is an external electromotive force. \mathbf{F}_u and \mathbf{F}_b are both solenoidal functions varying randomly and independently in time with time correlation τ . \mathbf{F}_u is acting only on wave numbers with $|\mathbf{k}| = k_u = 2$ and is nonhelical: $\langle \mathbf{F}_u \cdot \nabla \times \mathbf{F}_u \rangle = 0$. \mathbf{F}_b is acting only in the largest scale of the system $|\mathbf{k}| = k_b = 1$, and in general has nonzero helicity. All the parameters of the runs can be found in Table I. For the simulations a pseudospectral code was used [21,22] on grids of size 512^3 (runs A1–A13) and 1024^3 (runs B1–B3).

In a typical helical run all quantities grow initially up to a point when dissipation rates and kinetic energy reach a steady state while the magnetic energy is still increasing slowly. During this time the magnetic field is composed of a large-scale helical component B_L with $|\mathbf{k}| \approx 1$ that contains most of the magnetic energy and small scale turbulent fluctuations b of amplitude $b \sim u$. Thus magnetic energy E_M provides a measure of the large-scale field $E_M \approx \frac{1}{2} B_L^2$, while kinetic energy E_K provides a measure of the turbulent fluctuations. The growth of B_L depends on the amplitude and the helicity of the magnetic forcing. The evolution of E_K and E_M of the large resolution runs can be seen in Fig. 1. Due to the slow increase of the magnetic energy it is possible to perform short time averages (over a few turn over times) and obtain global averaged quantities for

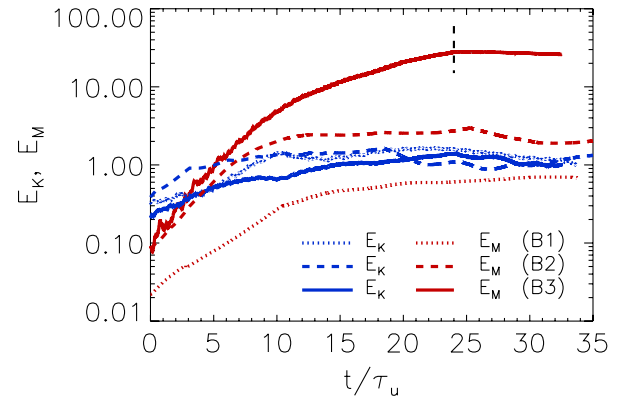


FIG. 1 (color online). Kinetic and magnetic energy evolution as a function of time for the three 1024^3 runs. The vertical dashed line indicates when the forcing parameters changed from the ones for B3' to the ones for B3.

various values of magnetic energy from the same run. Thus the turbulent scaling of the energy dissipation rate can be tested using multiple measurements for a wide range of magnetic field strength that here is quantified by $\mu \equiv E_M/E_K$. The system is statistically isotropic (there is no preferred direction if an ensemble average or long time average is considered) that allows us to perform spherical averages and thus improve two point statistics compared to the case with uniform magnetic fields. We note however that a single “snapshot” of the field can be very anisotropic.

Figure 2 shows the energy dissipation rate normalized by $U_{\text{rms}}^3 k_u = (2E_K)^{3/2} k_u$ (top panel) and the ratio of Ohmic to viscous dissipation (bottom panel) as a function of the energy ratio μ for all the examined runs. The data cover more than two decades of the parameter μ . While little variation is observed for the ratio $\epsilon_\eta/\epsilon_\nu$, three different behaviors can be observed for the total energy dissipation rate. First, over the range μ ($0.5 \leq \mu \leq 20$) the energy dissipation is independent of μ . This implies that ϵ follows the Kolmogorov scaling $\epsilon \propto u_\ell^3/\ell$ even when the large-scale magnetic energy is twenty times greater than the turbulent kinetic energy. The data include runs that vary

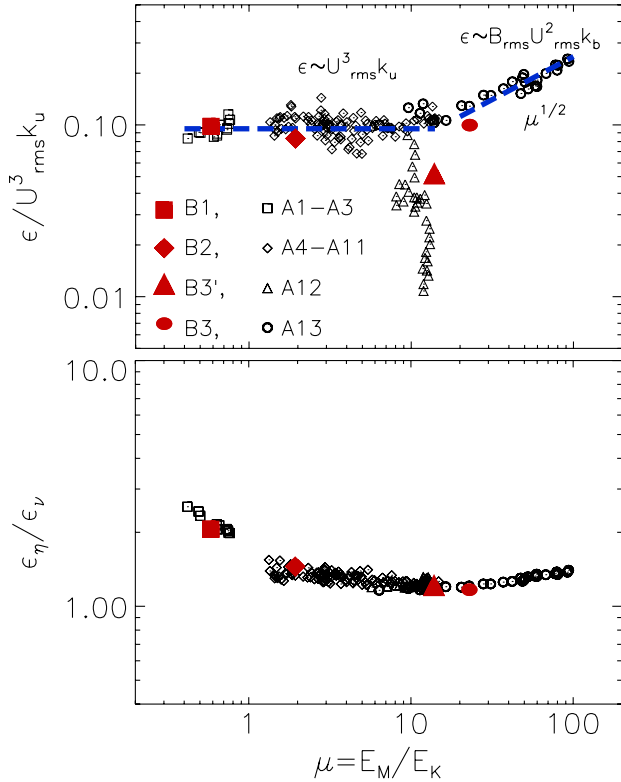


FIG. 2 (color online). Top panel: The energy dissipation rate ϵ normalized by $U_{\text{rms}}^3 k_u$ as a function of $\mu = E_M/E_K$ for all runs. $B_{\text{rms}} = \sqrt{2E_M}$ and $U_{\text{rms}} = \sqrt{2E_K}$. The dashed lines indicate the scaling $\epsilon \propto U_{\text{rms}}^3 k_u$ and $\epsilon \propto U_{\text{rms}}^2 B_{\text{rms}} k_b \propto \mu^{1/2}$. Bottom panel: The ratio of Ohmic dissipation rate $\epsilon_\eta = \eta \langle |\nabla b|^2 \rangle$ to the viscous dissipation rate $\epsilon_\nu = \nu \langle |\nabla u|^2 \rangle$ as a function of E_b/E_u .

from fully helical to nonhelical, and strongly magnetically forced to dynamo runs and for $\mathcal{R}_\lambda \sim 100$ to $\mathcal{R}_\lambda \sim 300$. Thus this result seems to be very general and robust in this range.

At μ larger than 10, two new branches appear. The results of run A12 that are fully helical and strongly magnetically forced are marked by triangles in Fig. 2. For this run both magnetic and kinetic energy is concentrated in the large scales building helical structures with very small turbulent fluctuations. Since they are both helical, the nonlinearities are minimized. As a result the large-scale magnetic and kinetic energy both increase with time keeping their ratio μ fixed while the small scale fluctuations and the dissipation rates saturate with time. As a result the normalized dissipation rate $\epsilon/U_{\text{rms}}^3 k_u$ decreases with time resulting in the behavior seen in Fig. 2. The dynamics here are controlled by magnetic helicity condensates, and despite the large Reynolds number they do not have finite dissipation ($\lim_{\text{Re} \rightarrow \infty} \epsilon > 0$). Thus they are not truly turbulent.

Run A13 marked by circles in Fig. 2 is strongly magnetically forced in order to achieve large values of μ within the time limitations imposed by the computational costs. This run, although in agreement with the turbulent scaling for $\mu \leq 20$, transitions to the scaling $\epsilon \propto \mu^{1/2}$ as indicated by the dashed line in the figure. This scaling can be understood if we consider that the main mechanism for cascading the injected energy is not the velocity shear $S_u \propto U_{\text{rms}} k_u$ but rather the magnetic shear $S_b \propto B_{\text{rms}} k_b$ that shreds Alfvén wave packets as they travel along chaotic magnetic field lines. The resulting scaling is $\epsilon \propto S_b U^2 \propto U^3 k_b \mu^{1/2}$ observed in Fig. 2. Thus the large-scale field rather than suppressing the turbulence cascade, it enhances it.

None of the runs showed a weak turbulence scaling that would have implied according to Eq. (2) the scaling $\epsilon \propto U_{\text{rms}}^4/B_L k_u \propto \mu^{-1/2}$. There are few possible interpretations for this result. First, just like the case of the uniform magnetic field, the absence of weak turbulence can be explained by the entrapment of energy in modes that vary perpendicular to the local magnetic field so that $\ell_\perp \ll \ell_\parallel$ makes the nonlinear coupling strong. Another possibility is the lack of uniformity of the magnetic energy density: regions exist in space with weak local magnetic field where eddies can be stretched with no resistance from magnetic tension. If the cascade in these regions dominates, the scaling of turbulence becomes independent of B_L . A final possibility is that magnetic instabilities reveal themselves altering the scaling (like run A13) before the magnetic field becomes strong enough for weak turbulence to manifest itself.

The energy spectra E_m, E_k for the high resolution runs B1, B2, B3 are shown in Fig. 3. For the B1 dynamo run the kinetic energy spectrum shows a power-law scaling slightly less steep than the $k^{-3/2}$ prediction. A clear change

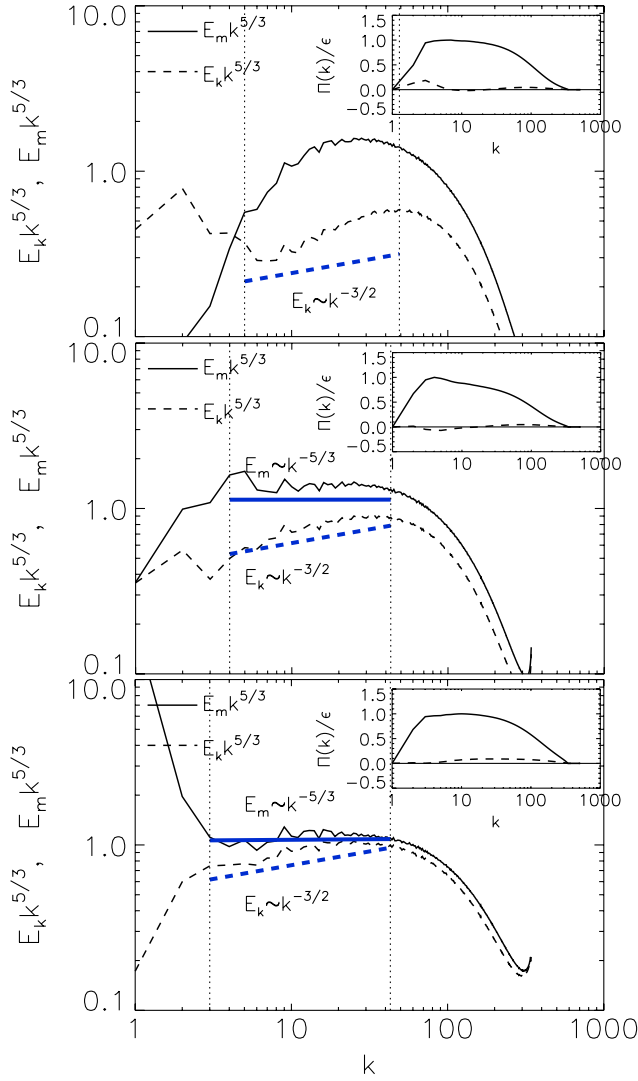


FIG. 3 (color online). Kinetic and magnetic compensated energy spectra for the runs *B1*, *B2*, *B3* (from top to bottom). The straight lines indicate the scaling $k^{-5/3}$ (solid line) and $k^{-3/2}$ (dashed line). The inset shows the energy flux $\Pi(k)$ (solid line) and $\Pi_u(k)$ (dashed line).

of slope at $k \sim 8$ where $E_m(k)$ becomes larger than $E_k(k)$ is also observed. The magnetic energy spectrum does not show a power-law scaling. The absence of a power-law scaling might be linked to the absence of large-scale magnetic structures due to the random forcing. The *B2*, *B3* runs, despite the one order of magnitude difference in μ , show similar results. The kinetic energy spectrum is well fitted by a $k^{-3/2}$ power law while the magnetic energy spectrum is best fitted by a $k^{-5/3}$ law. These values are also observed in the velocity and magnetic field spectra in the solar wind [23–25]. This agreement on the spectrum exponents (despite the absence of a guiding field in our simulations) suggests that effects like the nonuniformity of the large-scale magnetic field can be important. Finally, we note that the presence of the two different exponents

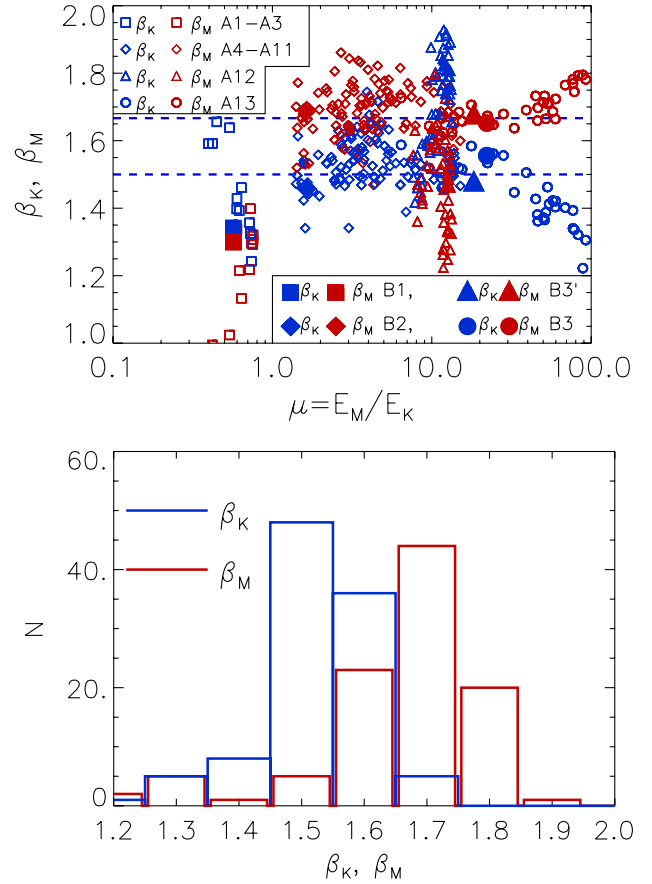


FIG. 4 (color online). Top panel: Measured exponents β_K and β_M for all runs. The exponents were calculated by a linear fit in the range $2k_u < k < \frac{3}{4}k_v$, where k_{nu} corresponds to the peak of the energy spectrum. Bottom panel: Distribution of the measured exponents for all runs in the range $1 < E_M/E_K < 20$, excluding run *A12* and *A1–A3*.

possibly indicates that a clear inertial range has not been reached yet, even at 1024^3 grid sizes. The insets in Fig. 3 show the total energy flux $\Pi(q) \equiv \langle \mathbf{u}_q^< (\mathbf{u} \cdot \nabla \mathbf{u} - \mathbf{b} \cdot \nabla \mathbf{b}) + \mathbf{b}_q^< (\mathbf{u} \cdot \nabla \mathbf{b} - \mathbf{b} \cdot \nabla \mathbf{u}) \rangle$ [26] (solid lines) and the energy flux due to the vortex stretching term $\Pi_u(q) \equiv \langle \mathbf{u}_q^< (\mathbf{u} \cdot \nabla \mathbf{u}) \rangle$ (dashed line). $\mathbf{u}_q^<$, $\mathbf{b}_q^<$ are the filtered velocity fields containing only wave numbers with $|\mathbf{k}| < q$. In all three cases the vortex stretching term plays a minor role in cascading the energy.

The top panel of Fig. 4 shows the measured power-law exponents from all the runs. The exponents were calculated by fitting power-law solutions $E_k \sim A_k k^{-\beta_K}$ and $E_m \sim A_m k^{-\beta_M}$ in the range $2k_u < k < \frac{3}{4}k_v$, where k_v corresponds to the peak of the enstrophy spectrum $k^2 E_k$. The range of fitting can be seen in Fig. 3 by the vertical dotted lines. The bottom panel shows the distribution of these exponents in the range $1 < \mu < 20$, excluding run *A12* and the *A–A3* dynamo runs. Although the dispersion of these values is quite large the exponents do not show much dependence on the amplitude of the magnetic field. Their values are

concentrated around $k^{-5/3}$ for the magnetic energy spectrum and $k^{-3/2}$ for the kinetic energy spectrum, in agreement with the high resolution runs.

Concluding, this work has showed the independence of (a) the normalized energy dissipation rate ($\epsilon \propto U_{\text{rms}}^3 k_u$) and (b) the spectral exponents ($\beta_M \approx 5/3$ and $\beta_K \approx 3/2$) on the amplitude of the large-scale magnetic field over a large range of μ and for a variety of forcing configurations. For very strong magnetic fields $\mu > 20$, the energy dissipation scaling transitioned to $\epsilon \propto B_{\text{rms}} U_{\text{rms}}^2 k_b$, implying that the cascade is driven by magnetic shear. The measured scaling of the energy dissipation is both fundamental (it can be applied in a variety of contexts) and nontrivial (it cannot be derived uniquely from dimensional arguments). Deviations were observed only for fully helical flows that formed magnetic helicity condensates in the large scales that do not follow a turbulent scaling. Analysis of higher order moments [26], local anisotropy, and scale interactions [27] might shed more light on the processes that control MHD turbulence.

This work was performed using HPC resources from GENCI-CINES (Grant No. 2012026421).

[1] G. I. Taylor, *Proc. R. Soc. A* **151**, 421 (1935).
 [2] G. K. Batchelor, *Theory of Homogeneous Turbulence* (Cambridge University Press, Cambridge, England, 1953).
 [3] A. Kolmogorov, *Dokl. Akad. Nauk SSSR* **31**, 583 (1941).
 [4] Y. B. Zeldovich, A. A. Ruzmaikin, and A. A. Sokoloff, *Magnetic Fields in Astrophysics* (Gordon and Breach, New York, 1990).
 [5] P. A. Davidson, *An Introduction to Magnetohydrodynamics* (Cambridge University Press, Cambridge, England, 2001).

[6] Y. Zhou, W. H. Matthaeus, and P. Dmitruk, *Rev. Mod. Phys.* **76**, 1015 (2004).
 [7] Y. Zhou and W. H. Matthaeus, *Phys. Plasmas* **12**, 056503 (2005).
 [8] Y. Zhou, *Phys. Rep.* **488**, 1 (2010).
 [9] S. V. Nazarenko, *Wave Turbulence* (Springer-Verlag, Berlin, 2011).
 [10] P. S. Iroshnikov, *Astron. Zh.* **40**, 742 (1963).
 [11] R. H. Kraichnan, *Phys. Fluids* **8**, 1385 (1965).
 [12] P. Goldreich and S. Sridhar, *Astrophys. J.* **438**, 763 (1995).
 [13] S. Boldyrev, *Phys. Rev. Lett.* **96**, 115002 (2006).
 [14] A. Bhattacharjee and C. S. Ng, *Astrophys. J.* **548**, 318 (2001).
 [15] S. Galtier, S. V. Nazarenko, A. C. Newell, and A. Pouquet, *J. Plasma Phys.* **63**, 447 (2000).
 [16] A. Beresnyak, *Phys. Rev. Lett.* **106**, 075001 (2011).
 [17] J. Mason, J. C. Perez, S. Boldyrev, and F. Cattaneo, *Phys. Plasmas* **19**, 055902 (2012).
 [18] J. C. Perez and S. Boldyrev, *Astrophys. J.* **672**, L61 (2008).
 [19] B. Bigot and S. Galtier, *Phys. Rev. E* **83**, 026405 (2011).
 [20] A. Alexakis, *Phys. Rev. E* **84**, 056330 (2011).
 [21] D. O. Gomez, P. D. Mininni, and P. Dmitruk, *Adv. Space Res.* **35**, 899 (2005).
 [22] D. O. Gomez, P. D. Mininni, and P. Dmitruk, *Phys. Scr.* **T116**, 123 (2005).
 [23] C. Salem, J.-M. Bosqued, D. E. Larson, A. Mangeney, M. Maksimovic, C. Perche, R. P. Lin, and J.-L. Bougeret, *Geophys. Res. Lett.* **106**, 21701 (2001).
 [24] J. J. Podesta, D. A. Roberts, and M. L. Goldstein, *Astrophys. J.* **664**, 543 (2007).
 [25] C. C. Salem, A. Mangeney, S. Bale, and P. Veltri, *Astrophys. J.* **702**, 537 (2009).
 [26] D. Biskamp, *Magnetohydrodynamic Turbulence* (Cambridge University Press, Cambridge, England, 2003).
 [27] A. Alexakis, P. D. Mininni, and A. Pouquet, *Phys. Rev. E* **72**, 046301 (2005).